JOURNAL OF THE ROYAL SOCIETY INTERFACE

Supporting information for:

Surface morphology enhances deposition efficiency in biomimetic, wind-driven fog collection

A. Shahrokhian, J. Feng & H. King

*Corresponding author email: hking@uakron.edu

This PDF file includes:

- Captions for Movies S1 to S3
- Supplementary Figs. S1 to S6

Videos. .

Movie S1- Flow past smooth vs. bumpy targets at $Re \sim 5000$. Addition of bumps appears to have no effect on separation point, wake size and boundary layer condition.

Movie S2- Close contact visualization of the flow past smooth and bumpy targets. While the bumpy target intercepts with more droplets, hydrodynamic interactions seem to impede collision of some, causing them to slide along contours of the bump. The video is slowed down 1000 times.

Movie S3- Time lapse video of fog collection for smooth and bumpy targets. The video is replayed at 10 times its original speed. More accumulation is observed in bumpy target compared to the smooth one. The accumulation of water droplets on the windward side of the bumps suggests direct impaction as opposed to circulation behind of the obstructions.

Data availability. The data presented in this work is available upon request.

Code availability. Code for the analysis described in data analysis section and other analyses presented in this paper are available upon request.

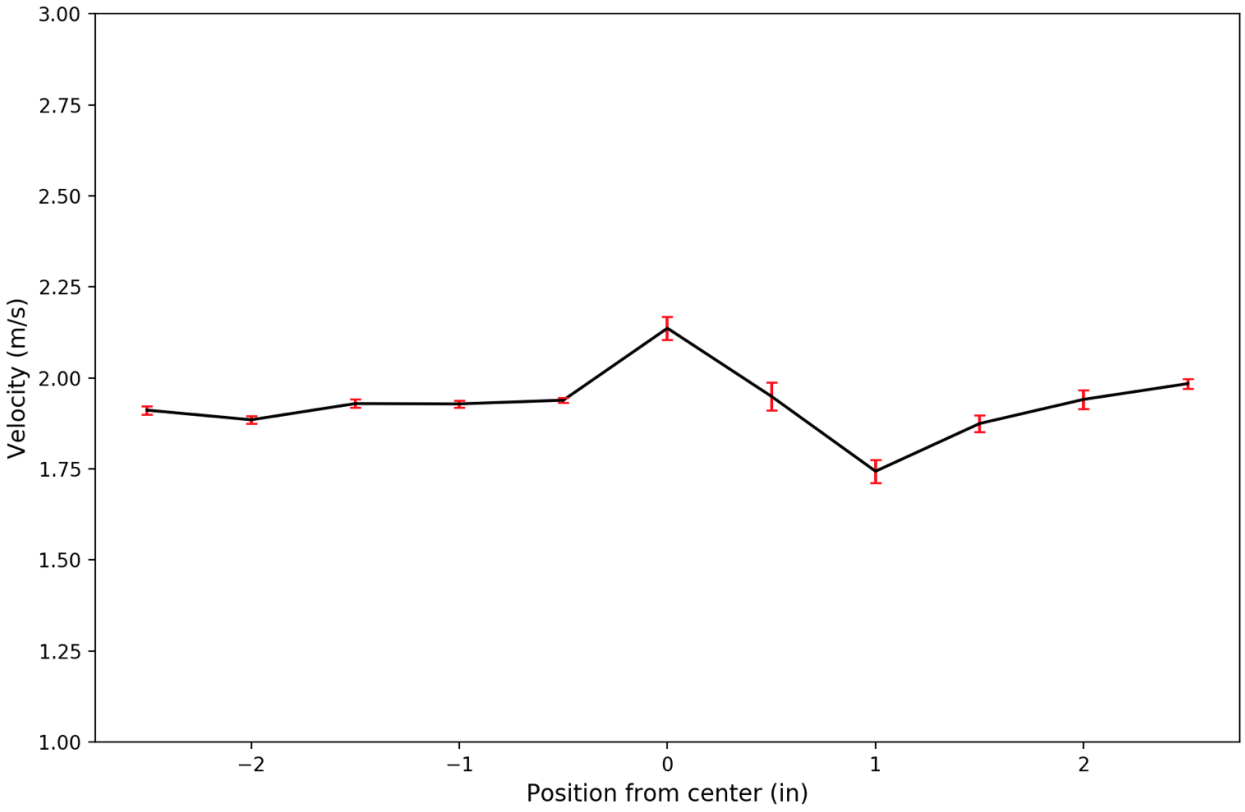

Fig.S 1: Velocity profile. Velocity profile across the test section of the wind tunnel was measured in every half an inch for 5 minutes using an anemometer (HHF1001A, OMEGA Engineering Inc.). The averaged values and the estimated values in between measurement locations are shown as a black line. $2m/s$ is considered as the average velocity across the section for calculations.

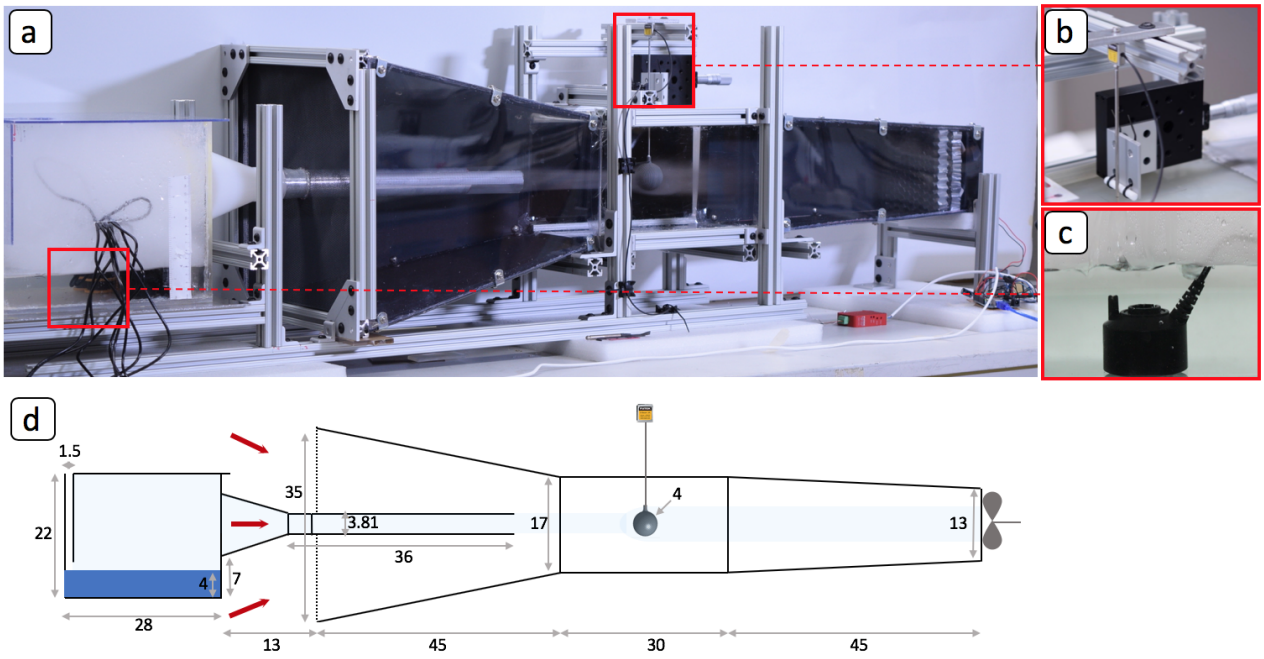

Fig.S 2: Wind tunnel specifications. a) The wind tunnel in operation. The flow direction is from left to right. b)A high-precision load cell is installed above the test section and connected to the target via a stainless-steel rod. The rod is supported from the leeward side by a Teflon rod (white) to cancel drag. c) Ultrasonic mist-makers (nebulizers) placed in the fog chamber are immersed in 4 cm of water. The water level is controlled using a pressure sensor. d) Schematic diagram of the wind tunnel for controlled fog application. The dimensions shown are in unit of centimeters.

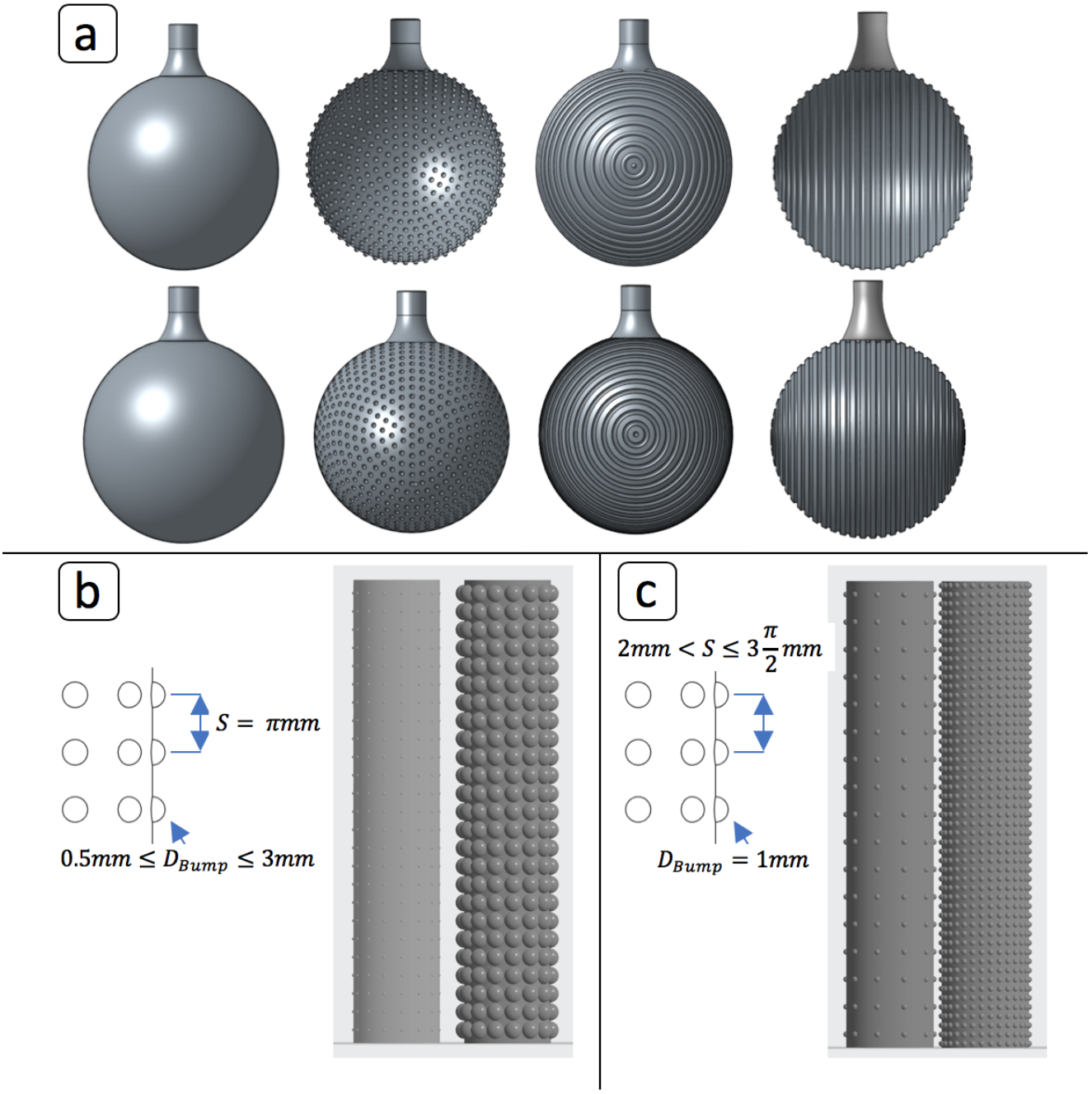

Fig.S 3: Fog collecting targets. a) 3D designs of spherical fog-capturing targets (diameter 40mm) two smooth, one bumpy, one dimpled, two grooved and two ridged. All features are $1mm$ diameter with $\sim\frac{2\pi}{3}mm$ center-to-center spacing. (b) Bumpy cylindrical targets with fixed spacing between bumps (center-to-center spacing of πmm) and varying bump diameters (from 0.5mm to 3mm). (c) Bumpy cylindrical targets with fixed bump diameter (1mm) and varying spacing between them (2mm to $3\pi/2$ mm).

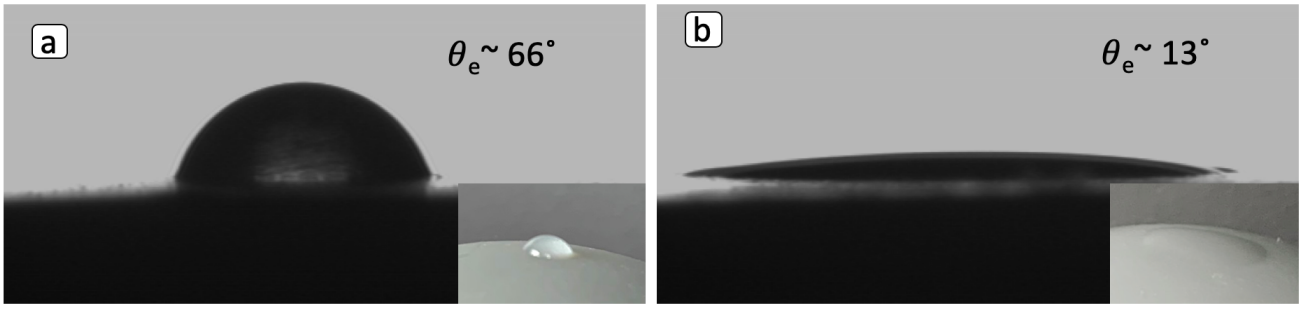

c

Sample	$\theta_a(^\circ)$	$\theta_r(^\circ)$
a (Not coated)	~ 80	~ 20
b (Coated)	~ 15	~ 10

Fig.S 4: Contact angle measurements. Water droplet static contact angles ($\sim\ 5\mu L$) on flat surface and on the spherical targets (inset) a) Grey04 (Not coated) b) Grey04 coated with anti-fogging solution. c) Advancing and receding contact angles for a and b.

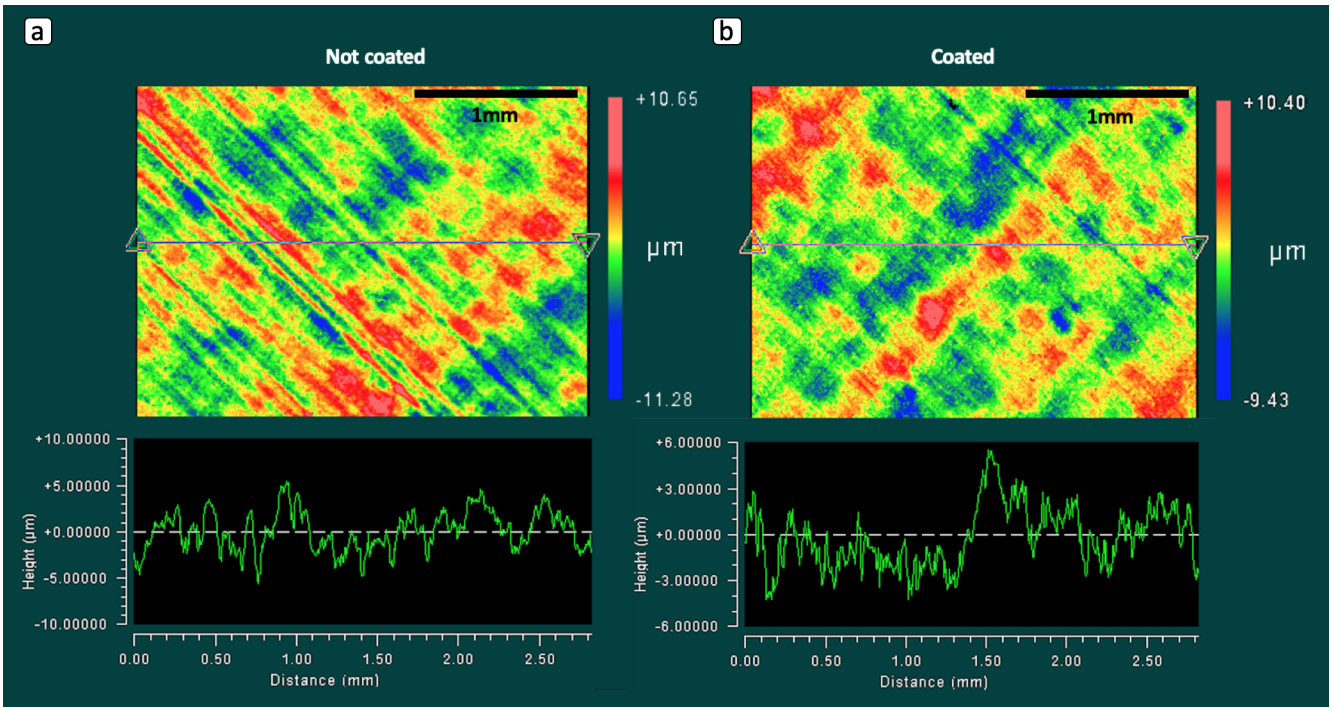

Fig.S 5: Surface roughness measurements. Surface roughness of 3D-printed slabs measured using 3D optical interferometer (Zygo New View 7300). a) Grey04 not coated, maximum peak to valley height $\sim 22\mu m$ ($RMS \sim 2.4\mu m$) b) Grey04 coated with anti-fogging solution, maximum peak to valley height $\sim 20\mu m$ ($RMS \sim 2.3\mu m$).

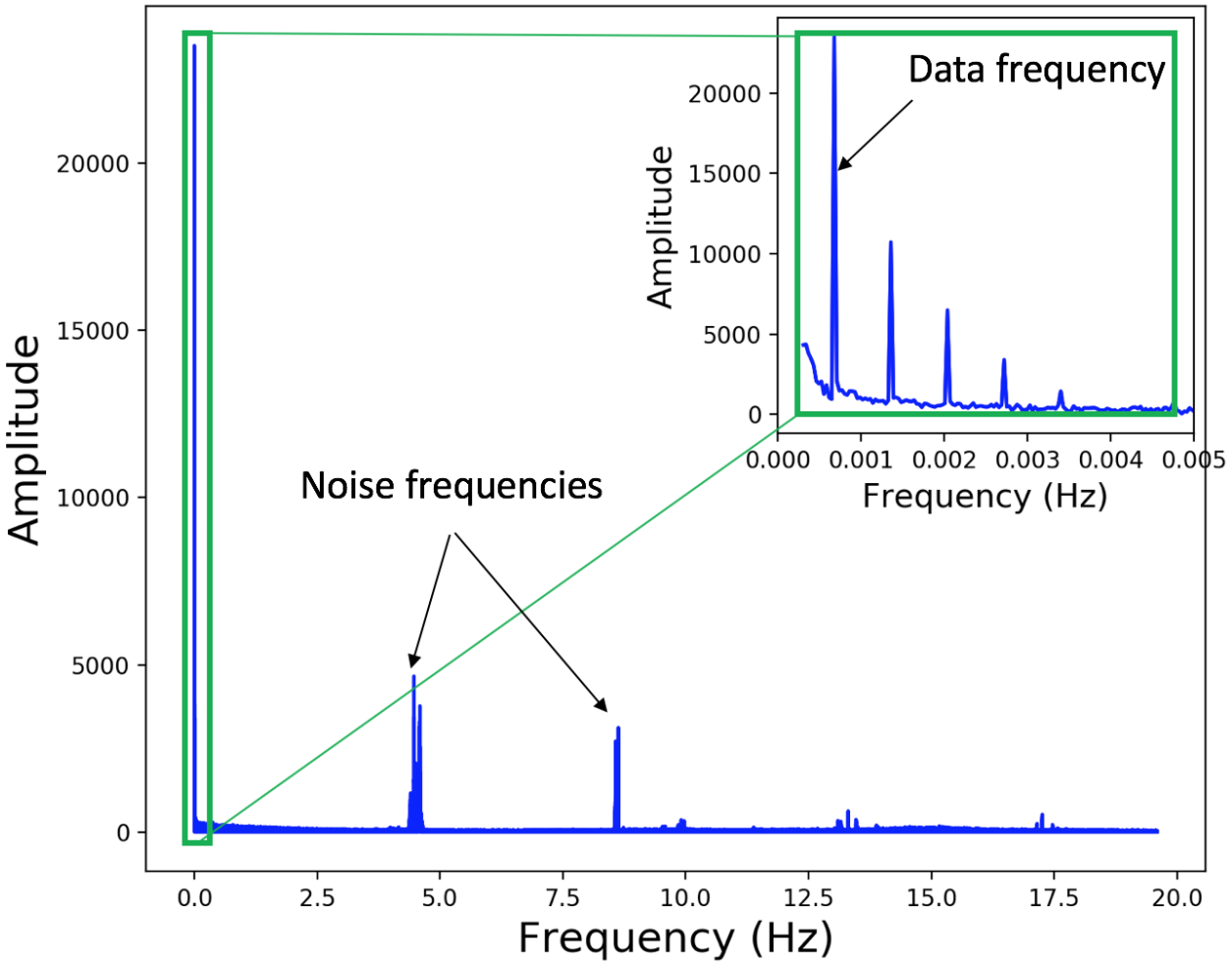

Fig.S 6: Fast Fourier transform of the data measured by the loadcell. The prominent peak is at 0.00069 Hz (period is 24 minutes) representing the frequency of data measurement. The harmonics of this signal are at 0.00138, 0.00207, 0.00276 and 0.00345 Hz. The peaks located at 4.6, 8.6, 9.9, 13.3 and 17.2 Hz correspond to noise frequencies. The y-axis represents the relative amplitude of the signals, not the actual amplitude.